# Ultrafast-based projection-reconstruction three-dimensional nuclear magnetic resonance spectroscopy

Mor Mishkovsky
*Department of Chemical Physics, Weizmann Institute of Science, 76100 Rehvot, Israel*

Eriks Kupče
*Varian Ltd., 28 Manor Road, Walton-on-Thames, Surrey KT12 2QF, United Kingdom*

Lucio Frydman[a)]
*Department of Chemical Physics, Weizmann Institute of Science, 76100 Rehvot, Israel*

(Received 2 April 2007; accepted 21 May 2007; published online 20 July 2007)

Recent years have witnessed increased efforts toward the accelerated acquisition of multidimensional nuclear magnetic resonance (*n*D NMR) spectra. Among the methods proposed to speed up these NMR experiments is "projection reconstruction," a scheme based on the acquisition of a reduced number of two-dimensional (2D) NMR data sets constituting cross sections of the *n*D time domain being sought. Another proposition involves "ultrafast" spectroscopy, capable of completing *n*D NMR acquisitions within a single scan. Potential limitations of these approaches include the need for a relatively slow 2D-type serial data collection procedure in the former case, and a need for at least *n* high-performance, linearly independent gradients and a sufficiently high sensitivity in the latter. The present study introduces a new scheme that comes to address these limitations, by combining the basic features of the projection reconstruction and the ultrafast approaches into a single, unified *n*D NMR experiment. In the resulting method each member within the series of 2D cross sections required by projection reconstruction to deliver the *n*D NMR spectrum being sought, is acquired within a single scan with the aid of the 2D ultrafast protocol. Full *n*D NMR spectra can thus become available by backprojecting a small number of 2D sets, collected using a minimum number of scans. Principles, opportunities, and limitations of the resulting approach, together with demonstrations of its practical advantages, are here discussed and illustrated with a series of three-dimensional homo- and heteronuclear NMR correlation experiments. © *2007 American Institute of Physics*. [DOI: 10.1063/1.2748768]

## I. INTRODUCTION

Multidimensional nuclear magnetic resonance (*n*D NMR) spectroscopy plays an increasingly central role in elucidating the structure and dynamics of complex chemical and biochemical systems.[1,2] These experiments can separate and correlate spin interactions along independent frequency domains, providing a spectral resolution and an information content unavailable in one-dimensional counterparts. One of the complications associated with implementing this kind of experiments lies in the relatively long times that, even in the absence of sensitivity constraints, are needed for completing the data acquisition. This is a consequence of the manner by which multidimensional NMR is traditionally implemented.[3–5] For instance in the specific three-dimensional (3D) NMR case on which the present study centers, signals along one of the dimensions—the so-called direct $t_3$ domain—are monitored over a few hundred milliseconds in the usual pulsed NMR fashion.[6] But the spins' evolution along the remaining indirect-domain time axes $(t_1,t_2)$ is indirectly monitored *via* a discrete incrementation of delays positioned throughout the pulse sequence, each of which will be associated with the collection of at least one independent scan. Numerous transients will therefore be needed for completing a proper sampling of the 3D NMR time domain regardless of sensitivity conditions, a complication that gets aggravated upon extending the experiment to higher dimensionalities.

Driven by this constraint and stimulated by an increasing reliance of structural determinations on high-dimensional ($\geqslant$3D) NMR experiments, a growing number of alternatives that depart from traditional *n*D NMR sampling principles, have began to emerge.[7,8] These routes include methods that process the data by non-Fourier methods,[9–12] acquisitions that incorporate frequency-based manipulations,[13] "accordioned" derivations[14] that increment multiple delays simultaneously,[15–17] and "ultrafast" methods based on encoding the spin evolution along spatial rather than temporal domains.[18,19] Each of these approaches has its respective advantages and disadvantages depending on factors such as the available per-scan sensitivity, the presence or absence of *a priori* spectral knowledge, the experimental speedup being sought, and hardware availability. The present study examines the possibilities opened up by bringing together two such methods, one based on projection-reconstruction (PR) NMR and the other on spatially encoded ultrafast acquisitions, into a single new protocol geared at the acquisition of high-dimensional NMR spectra. Such combination exhibits

[a)]Electronic mail: lucio.frydman@weizmann.ac.il

 

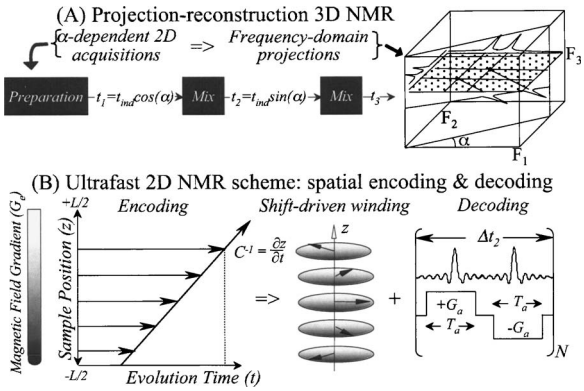


FIG. 1. Basic elements comprising the ultrafast 3D projection-reconstruction NMR approach. (A) Generic 3D PR sequence, whereby the indirect-domain parameters $t_1$ and $t_2$ are simultaneously incremented according to $t_1=t_{\mathrm{ind}}\cos(\alpha)$, $t_2=t_{\mathrm{ind}}\sin(\alpha)$, and the resulting data are then "back-projected" within the $F_1F_2$ domain into full 3D NMR spectra. (B) Principles of ultrafast 2D NMR, enabling one to probe the full extent of interactions between indirect and direct domains within a single scan by means of gradient-assisted spatial manipulations. See text for further details.

positive aspects, and opens up new spectroscopic alternatives absent to either PR or ultrafast NMR.

## II. PRINCIPLES OF SPATIALLY ENCODED 3D PROJECTION-RECONSTRUCTION NMR

We shall here focus on the new protocol as applied to the speeding up of 3D PR NMR experiments, by relying on a variety of approaches that collect the 2D NMR data making up the different projections required by the algorithm within a single scan. As a reminder, 3D PR NMR shortens the time required to complete the NMR acquisitions by substituting the nested incrementations of the indirect-domain evolution times $(t_1,t_2)$, with a limited number of 2D NMR acquisitions representing different projections of the spectral data within its 3D space. Such projections are then inverse Radon transformed for each discrete direct-domain $F_3$ frequency, to yield the full $F_1F_2F_3$ 3D spectrum being sought. The projected planes needed by this protocol can be collected in a number of ways; in the present case, we shall rely on the approach introduced in Ref. 17, whereby 2D time-domain signals are recorded with $t_1$ and $t_2$ parameters varied simultaneously at ratios defined by

$$t_1 = t_{\mathrm{ind}}\cos(\alpha), \quad t_2 = t_{\mathrm{ind}}\sin(\alpha), \tag{1}$$

over a series of increments $0 \leqslant t_{\mathrm{ind}} \leqslant t_{\mathrm{ind}}^{\max}$. $\alpha$ then becomes the angle subtended by different cross sections of the 3D time domain along a $(t_1,t_2)$ line defined by $\tan(\alpha)=\Delta t_2/\Delta t_1$ [Fig. 1(A)]. It follows from the Fourier slice-projection theorem[20] that a dense volume within the 3D time domain can be scanned by suitably varying the two indirect-domain parameters $t_{\mathrm{ind}}$ and $\alpha$, followed in either case by a conventional data acquisition along $t_3$. When cast in these terms not much seems to have been gained by PR-based methods over conventional 3D NMR acquisitions, as they still require the systematic incrementation of two parameters, $(t_{\mathrm{ind}},\alpha)$, instead of $(t_1,t_2)$. The discrete and sparse nature of peaks within typical 3D NMR frequency domains, however, implies that peak positions in the $F_1F_2F_3$ space can be identified using few $\alpha$ projections, in many cases as little as three. 3D (and in general $n$D) NMR acquisitions can thus be shortened substantially vis-à-vis conventional Fourier-based experiments, even if still requiring the acquisition of independent 2D cross sections in the combined $(t_{\mathrm{ind}},t_3)$ domain to properly define each the individual spectral frequencies.

To further accelerate 3D PR NMR experiments we propose collecting each of its constituent 2D cross sections in an ultrafast manner, suitably modified so as to encode multiple indirect domains along a single spatial axis. As summarized in Fig. 1(B) for a 2D NMR scenario, spatial encoding is a procedure which allows one to parallelize the serial incrementation of the time parameters involved in the pulse sequence, making it possible to collect the equivalent of a complete two-dimensional data set in a single scan.[18] Within the context of high resolution NMR such spatial encoding is most conveniently imparted by applying suitably refocused $G_e$ magnetic field gradients along the $z$ direction, in combination with a train of discrete or continuous frequency-selective radio frequency (rf) pulses exciting/inverting spins sequentially over a sample of length $L$ during a time period which (for consistency with the PR notation) we denote $t_{\mathrm{ind}}^{\max}$. The goal of spatial encoding is to create a "proportionality" between the indirect-domain evolution times of the spins and their positions throughout the sample, dictated by a spatiotemporal coefficient $C_{\mathrm{ind}}=dt_{\mathrm{ind}}/dz \approx t_{\mathrm{ind}}^{\max}/L$ under our control. The indirect-domain $\Omega_{\mathrm{ind}}$ frequencies to be measured imprint then a spatial winding on the spin coherences given by evolution phases $\phi_e(z)=C_{\mathrm{ind}}(z+L/2)\Omega_{\mathrm{ind}}$, which when considered over the full sample leads to no observable signal. Data detection in these experiments, however, is normally carried out as a function of time while oscillating an acquisition gradient $G_a$ that introduces an additional evolution term $[\gamma_a\int_0^{t_2}G_a(t')dt']z=kz$; this leads to a train of observable echoes whenever $k=-C_{\mathrm{ind}}\Omega_{\mathrm{ind}}$ whose Fourier transform as a function of the acquisition time reveals the full 2D NMR spectrum being sought, within a single scan. Moreover it has been shown that, if multiple spin evolutions are encoded along linearly independent geometries, an arbitrarily high number of independent time domains can be incorporated into such ultrafast scheme.[21] Although this provides a route for the single-scan collection of $n$-dimensional $(n \geqslant 3)$ NMR spectra, acquisitions of this kind demand two or more orthogonal gradients as well as intense signals in order to enable the complete characterization of all domains. As such conditions are not always met (for instance, when dealing with cryogenically cooled probeheads that at the moment offer a route to the acquisition of highest-sensitivity NMR data), we focus here on PR alternatives that accelerate the acquisition of high resolution 3D NMR spectra on the basis of single-scan 2D acquisitions, relying on a single $z$-axis gradient.

Merging the 3D PR and ultrafast 2D NMR principles involves translating the joint temporal incrementation conditions underlying the original projections, into analogous spatiotemporal terms. Assuming that the full sample length $L$ is employed for applying the joint indirect-domain $(t_1,t_2)$ encoding, this is equivalent to casting the original conditions in Eq. (1) into

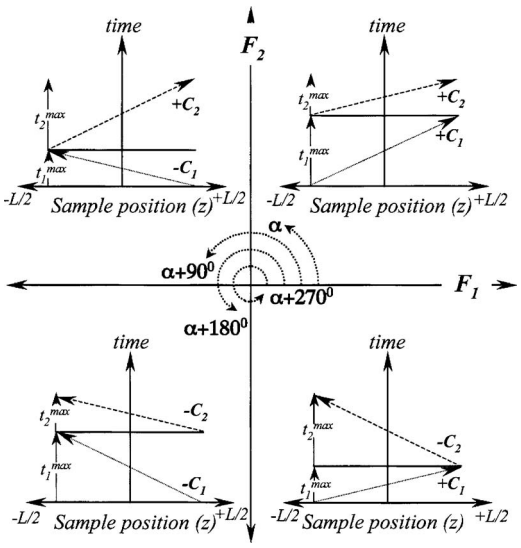


FIG. 2. Adapting the spatial encoding strategy to explore all four quadrants of the $F_1F_2$ indirect-domain spectral space. Each indirect domain is characterized by spatiotemporal coefficients $C_1$ and $C_2$, given by the spatial derivatives of the evolution times $t_1=t_{\mathrm{ind}}\cos(\alpha)$ and $t_2=t_{\mathrm{ind}}\sin(\alpha)$. The actual signs of $C_1$ and $C_2$ are determined by the sense chosen for the spins' spatial manipulation, which can proceed from the bottom of the sample up or vice versa. This sense can in turn be controlled either by choosing the rf sweep direction for a given gradient configuration, or by keeping a constant sense for the rf sweep but changing the encoding gradient's sign. As a result of these choices, accessing the full $0°\leqslant\alpha\leqslant 360°$ range of values becomes possible.

$$C_1 = C_{\mathrm{ind}}\cos(\alpha), \quad C_2 = C_{\mathrm{ind}}\sin(\alpha). \tag{2}$$

A point to notice is that by contrast to the positive-valued time parameters entailed in Eq. (1), signs in the $\{C_i\}_{i=1,2}$ coefficients of Eq. (2) can be chosen freely, depending on the $z$ direction toward which the spatial encoding progresses. This choice plays a role in the spatially encoded version of the PR reconstruction process, as it enables one to measure either sums or differences between the $\Omega_1$, $\Omega_2$ frequencies characterizing each indirect domain. Measuring a sum of such frequencies is analogous to measuring data from $\alpha$ projections lying in the first and/or third quadrants of the 2D indirect-domain $F_1F_2$ space, whereas their difference represents measurements in the second and/or fourth quadrants. In order to characterize these tilted projections unequivocally, further differentiations are needed between the first/third as well as between the second/fourth quadrants. A manner by which this distinction can be done derives from the $dt_{\mathrm{ind}}/dz$ definition given for the spatiotemporal coefficients, and which implies that carrying out a particular spatial encoding from the bottom of the sample upwards or from the top of the sample downwards can provide opposite $C$ signs and thereby the freedom needed for distinguishing among all different quadrants within the $F_1F_2$ space (Fig. 2). When translated in terms of the spatial patterns that are imposed on the NMR spin coherences, these possibilities allow one to create a helical winding along the $z$ direction whose overall phase is given by

$$\begin{aligned}\phi_e^{\mathrm{total}}(z) &= \phi_e^1(z) + \phi_e^2(z) \\ &= C_{\mathrm{ind}}\cos(\alpha)\Omega_1(z+L/2) \\ &\quad + C_{\mathrm{ind}}\sin(\alpha)\Omega_2(z+L/2).\end{aligned} \tag{3}$$

The 2D spectra stemming from this combination upon applying the usual $k$-driven ultrafast decoding will reveal, for different $\alpha$ values, peaks positioned according to

$$\Omega_{\mathrm{ind}}(\alpha) = \Omega_1\cos(\alpha) + \Omega_2\sin(\alpha) \tag{4}$$

as required by the original PR scheme. The following section demonstrates a number of different homo- and heteronuclear implementations of this kind of experiments, chosen to illustrate the diversity and flexibility that arise in their execution.

## III. EXPERIMENTAL EXAMPLES OF SPATIALLY ENCODED 3D PROJECTION-RECONSTRUCTION NMR

### A. PR NMR by concatenation of multiple real-time, spatially encoded modules

A number of variants have been proposed for executing the spatial encoding underlying ultrafast 2D NMR. These include discrete excitation/refocusing schemes,[19] as well as continuous frequency-swept strategies relying on either constant- or real-time,[22,23] amplitude- or phase-modulated modalities.[24,25] In principle any of these strategies could be concatenated along the guidelines formulated in the preceding section to yield the accordioned $(t_1,t_2)$ evolution required by PR; moreover, new spatial encoding alternatives also arise in this 3D case. We begin this survey with an example [Fig. 3(A), left] linking two spatially encoding blocks which, although different from one another, share a reliance on a dual-sweep, real-time modulation of the $(\Omega_1,\Omega_2)$ interactions. The first of these spatial encoding blocks employs a pair of identical chirped rf pulses imparting net $\pi/2$ nutations over a delay $t_1^{\mathrm{eff}}=2t_1^{(\pi/2)}$, applied in the presence of $\pm G_e^1$ gradients with opposite polarities.[22] The spin excitation and storage executed by these two pulses lead to a coherence pattern of the form $\cos[\phi_e^1(z)+\theta^1]$: an amplitude-modulated spatial winding. For encoding the second indirect time domain we chose a phase-modulated approach made of a swept $\pi/2$ pulse applied over a time $t_2^{(\pi/2)}$ in the presence of a gradient $G_e^2$, followed by a swept inversion $\pi$ pulse of duration $t_2^{(\pi)}$ under a gradient $G_e^{2\prime}$. As detailed elsewhere this will lead to a linear $z$ encoding, provided that the timings and gradient strengths employed in the sweeps fulfill the condition $G_e^2 t_2^{(\pi/2)}=2G_e^{2\prime}t_2^{(\pi)}$.[24,25] Given our choice of equally signed $G_e^2$ and $G_e^{2\prime}$ gradients, a phase-modulated pattern of the form $\exp\{i[\phi_e^2(z)+(G_e^2 t_2^{(\pi/2)})z/2]\}$ results, characterized by an encoding time $t_2^{\mathrm{eff}}=2t_2^{(\pi)}-t_2^{(\pi/2)}$ and by an additional $G_e^2 t_2^{(\pi/2)}$-derived linear winding.

In order to combine these two spatial encoding elements into a series of $\alpha$-incremented PR experiments, an overall duration $t_{\mathrm{ind}}^{\max}$ parameter needs to be defined, and the relative extent of each spatial encoding delay defined above incremented according to the conditions set by Eqs. (1) and (2): $t_1^{\mathrm{eff}}=\cos(\alpha)t_{\mathrm{ind}}^{\max}$, $t_2^{\mathrm{eff}}=\sin(\alpha)t_{\mathrm{ind}}^{\max}$. The fact that the first of these encoding processes involves a magnetization storage and that a gradient-derived shift occurs during the second, leads to an

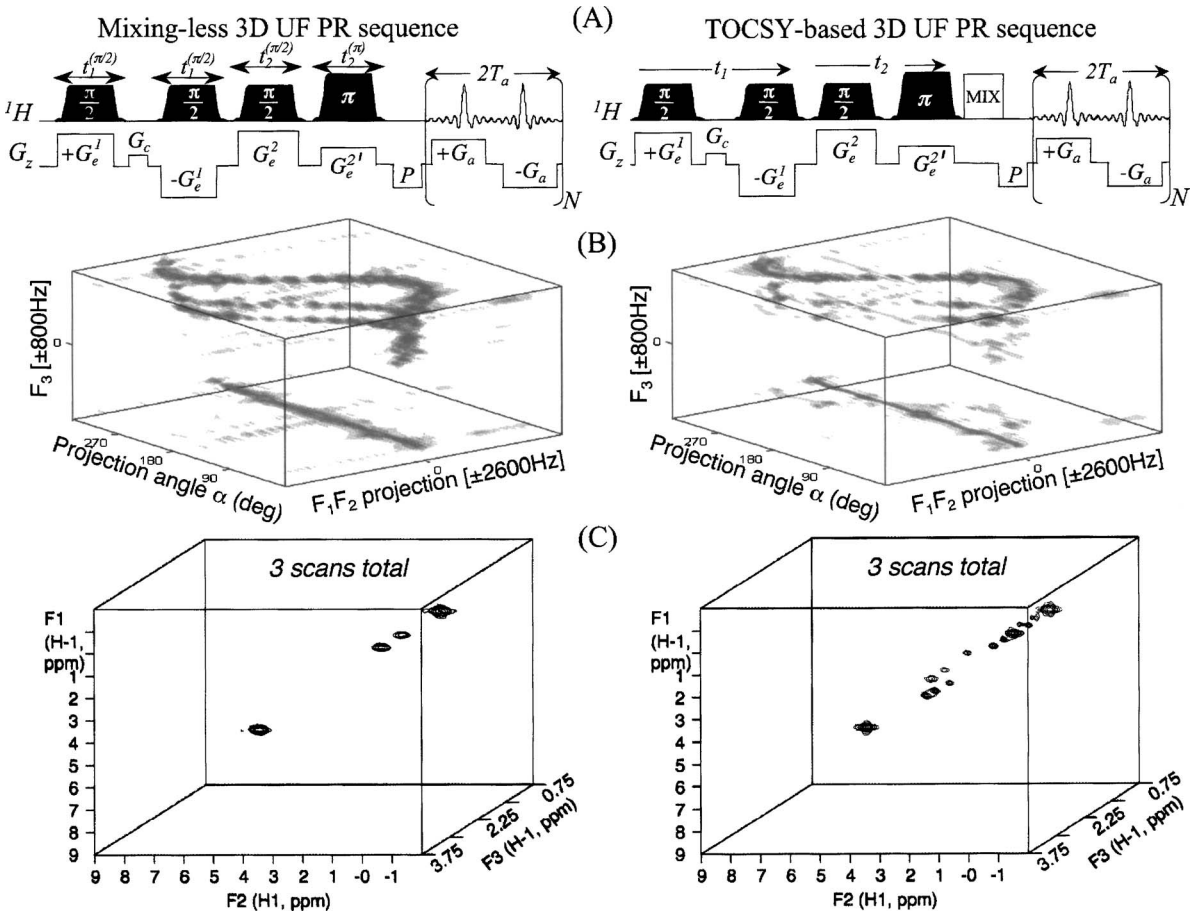


FIG. 3. Ultrafast 3D homonuclear PR NMR tests on an *n*-buthylchloride/$CDCl_3$ sample. (A) Pulse sequences without (right) and with (left) an isotropic mixing period inserted between the $t_2$ encoding and the $t_3$ acquisition. In all cases the first indirect domain is encoded with an amplitude modulation block whereas the second is encoded using a phase-modulated scheme, both of them proceeding in real time. Coherence pathway selection during $t_1$ proceeds thanks to the windings imparted by $G_c$ and by $G_e^2$; a purging gradient pulse (P) of strength $-G_a$ and duration $T_a/2$ is also used to shift the $k=0$ (i.e., $\Omega_{\text{ind}}=0$) position to the center of the $T_a$ sampling window. Details on the sequence operation are given in the text; other experimental parameters include $G_e^1=10$ G/cm, $G_c=\pm 50$ G/cm with duration set according to $t_{\text{ind}} \sin\alpha/10$ (to compensate for the $G_e^2$-incurred dephasings), $t_{\text{ind}}^{\max}=10$ ms, $G_e^2=10$ G/cm, $G_e^{2\prime}=5$ G/cm, $G_a=25$ G/cm, $T_a=300$ $\mu$s, $N=128$, 40 ms DIPSI-2 mixing (Ref. 31). Like all remaining examples shown in this study these tests were run on a Varian iNova® NMR spectrometer and probe operating at a 501 MHz Larmor frequency using a single-axis gradient setting. (B) Sinograms arising from each of the pulse sequences, displaying for each $F_3$ peak unique trajectories according to $\Omega_1 \cos\alpha + \Omega_2 \sin\alpha$. The straight line at the bottom of the "cube" corresponds to the on-resonance $\Omega_1=\Omega_2=0$ case and therefore shows no modulation with the projection angle. (C) Full 3D spectra reconstructed from three $\alpha$ projections (210°, 240°, and 270°) as described in Ref. 17 (in the right-hand plot, cross peaks are to be looked for in the dimension "perpendicular" to the page).

overall spin coherence pattern

$$S(z) \propto \cos[\phi_e^1(z) + \theta^1]\exp\{i[\phi_e^2(z) + (G_e^2 t_2^{(\pi/2)})z/2 + \theta^2]\}. \tag{5}$$

This signal is not exactly desired, as it contains an amplitude $t_1$ modulation leading to a projection depending on $\pm\cos(\alpha)$, and a phase-modulated $t_2$ encoding that in addition to the desired $\phi_e^2(z)$ behavior includes a strong $G_e^2$-dependent winding of the coherences. A known solution to deal with ambiguities arising from cosine-type amplitude modulations consists of relying on pairs of gradient pulses that can select a particular coherence transfer pathway during $t_1$.[1,2,26] In the present instance, the post-$t_1$ $G_e^2 t_2^{(\pi/2)} z/2$ winding can take the role of one such gradient pulses. All that was needed to transform the $t_1$ amplitude modulation into the desired phase-modulated form was thus the inclusion of a suitable [i.e., of a $G_e^2 t_2^{(\pi/2)}$ dependent] $G_c$ coherence selection gradient within this indirect domain. Such precaution enabled us to select arbitrary $\alpha$ projection angles conforming to $C_{\text{ind}}[\Omega_1 \cos(\alpha) + \Omega_2 \sin(\alpha)](z+L/2)$ into the spatial winding. In addition to $G_c$ a second ancillary gradient pulse ($P$) was included in all sequences, in order to shift the $\Omega_{\text{ind}}=0$ position to the center of the $k$ acquisition window and thus allow us to fully characterize positive and negative $\Omega_{\text{ind}}$ frequency modulations.

Figure 3(B) illustrates, for mixingless and TOCSY-based homonuclear 3D PR experiments on a *n*-buthylchloride/$CDCl_3$ solution, representative results arising from these sequencing considerations. Note that for each resonance along $F_3$, cross peaks in the orthogonal $F_1F_2$ domains describe the expected $\Omega_1 \cos(\alpha) + \Omega_2 \sin(\alpha)$ sinusoidal oscillation over a full $0 \leqslant \alpha \leqslant 360°$ range of rotations. In practice, the actual 3D NMR spectrum being sought can be reconstructed using a small subset of these single-scan projections. Figure 3(C) illustrates this by showing 3D "boxes" arising from these sequences and incorporating solely three projections out of the full sinogram set. In these cases, an effective experimental time of merely 4 s was required for arriving to each full 3D NMR spectrum.

### B. 3D PR NMR by concatenation of constant-time phase-modulated modules

A strategy like the one just illustrated for homonuclear correlations can be extended to heteronuclear cases, for instance, to HSQC or HMQC NMR experiments.[2] In cases like HSQC one could also differentiate $\pm\Omega_{\mathrm{ind}}$ frequencies by employing principles akin to those underlying the sensitivity enhancement versions of the experiment.[27] As a reminder, these strategies are meant to preserve the two orthogonal $2H_zI_x$, $2H_zI_y$ antiphase components resulting from a heteronuclear evolution; by altering the rf phases $\phi$ used to trigger the double-INEPT blocks of these sequences, one can thus distinguish $+\Omega$ from $-\Omega$ indirect-domain modulation frequencies. Implementing such sensitivity-enhanced procedures requires the creation and preservation of both orthogonal antiphase terms and thereby the use of a phase-modulated approach. The present section exemplifies this motif as applied to spatially encoded 3D heteronuclear PR NMR spectroscopy, incorporating constant-time rather than real-time phase modulation blocks.

A constant-time phase-modulated spatial encoding can be imparted by applying dual frequency-swept RF $\pi$ pulses, while in the presence of encoding gradients $\pm G_e$ of opposing signs.[23] Figure 4(A) illustrates how such pair of adiabatic passages can be incorporated into a sequence designed to do an ultrafast-based 3D PR NMR experiment, built around $^1$H–$^1$H 2D TOCSY and $^1$H–$^{15}$N 2D HSQC modules. Note that in addition to the phase-modulated sensitivity-enhanced route just described, this sequence also incorporates a pair of coherence selective gradients ($G_c$) before the first INEPT and prior to the final data acquisition blocks, in order to choose the absolute sign imparted by the $\Omega_I$ modulation. Figure 4(B) illustrates results arising upon relying on this pulse sequence to obtain two orthogonal 2D projections of the 3D data set, using a mixture of $^{15}$N-FMOC-Ala and $^{15}$N-FMOC-Val dissolved in $CDCl_3$ as target. The $\alpha=0°$ set corresponding to an $F_1F_3$ projection of the 3D spectral data presents a pure 2D $^1$H TOCSY correlation, whereas the $\alpha=90°$ set shows a pure $^{15}$N–$^1$H $F_2F_3$ HSQC correlation. Figure 4(C) presents the full $0° \leqslant \alpha \leqslant 360°$ rotation plots that can be separated for each $F_3$ peak in the mixture, illustrating a characteristic $\Omega_1 \cos(\alpha)+\Omega_2 \sin(\alpha)$ sinogram within the $F_1F_2$ domain. Once again, and as in the homonuclear case, the full 3D spectrum can be reconstructed using very few projections; Fig. 4(D) shows the results stemming from utilizing just three planes corresponding to $\alpha=0°$, 30°, and 90°. Each $^{15}$N peak in $F_2$ is correlated here to two different protons in $F_1$, one arising from the directly bound $H^N$ and the other from the $H^\alpha$.

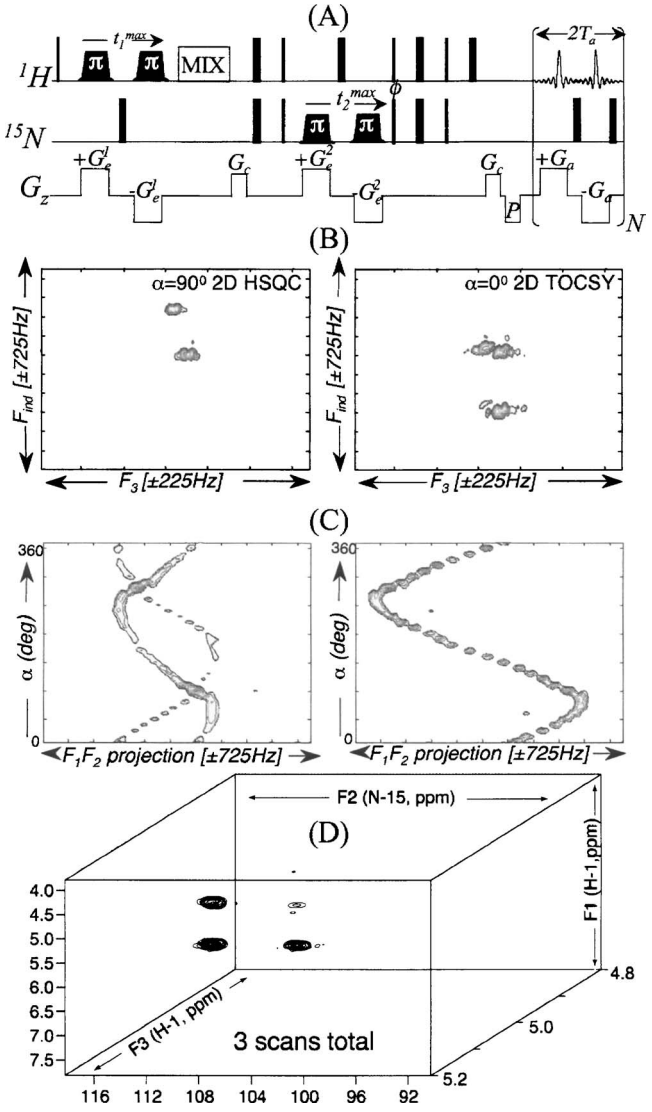


FIG. 4. Heteronuclear $^1$H–$^{15}$N–$^1$H ultrafast 3D PR tests on a $^{15}$N-FMOC-Ala/$^{15}$N-FMOC-Val $CDCl_3$ solution. (A) TOCSY-HSQC sequence encoding along the $z$ spatial dimension both indirect domains, by using a constant-time $\pi$-pulse based approach. The duration of each encoding block was determined according to $t_1^{\max}=t_{\mathrm{ind}}^{\max}\cos(\alpha)$, $t_2^{\max}=t_{\mathrm{ind}}^{\max}\sin(\alpha)$. Differentiation between $\pm\Omega_1$ frequencies was carried out using a coherence selective gradient $G_c$, whereas distinction between $\pm\Omega_2$ frequencies was done by altering the phase $\phi$ of the sensitivity-enhanced HSQC block between $\pm x$. As before, a purging gradient $P$ was introduced for shifting the frequency origin of the indirect domain. Narrow and wide lines denote broadband $\pi/2$ and $\pi$ pulses, separated in all cases by $(4J_{\mathrm{NH}})^{-1}$ delays. Additional experimental parameters: $G_e^{(1)}=10$ G/cm, $G_e^{(2)}=26$ G/cm, $t_{\mathrm{ind}}^{\max}=10$ ms, $G_c=\pm 20$ G/cm, $T_a=1$ ms, $G_a=3.5$ G/cm, $N=46$, $P=0.5$ ms at −3.5 G/cm, 20 ms DIPSI-2 mixing. (B) Orthogonal projections corresponding to the pure TOCSY ($\alpha=0°$) and $^{15}$N-HSQC ($\alpha=90°$) $F_{\mathrm{ind}}F_3$ 2D planes. (C) Rotation plots presented as 2D planes for each one of the $F_3$ peaks, demonstrating their respective sinusoidal trajectories over the full $0° \leqslant \alpha \leqslant 360°$ range. (D) Full 3D spectrum reconstructed from three projections and showing each $^{15}$N peak ($F_2$) correlated to two different protons ($F_1$): one arising from the directly bound $H^N$ and the other from the $H^\alpha$. The different intensities of the $H^\alpha$ cross peaks originate from differences between the $J(H^N-H^\alpha)$ coupling constants of the two amino acids.

### C. 3D PR NMR by merging single sweep, phase-modulated modules

The ultrafast-based 3D implementations illustrated so far concatenated a series of independent 2D spatial encoding modules. The fact that the 3D PR protocol relies on two indirect-domain encoding stages affecting the same $z$ coordinates, however, also opens up new spatial encoding alternatives unavailable in conventional ultrafast 2D acquisitions. This paragraph discusses one such new strategy capable of affording the spatial winding pattern expected by PR, illustrated with homonuclear 3D correlations of the kind discussed in Sec. III A.

The approaches presented in Figs. 2–4 implement a con-

tinuous spatial encoding of the spin interactions along each of the encoded indirect domains, using dual rf sweeps under the effects of two different gradients. This is needed to distinguish the frequency shifts generated by the external field gradient from those arising from the internal interactions and leave at their conclusion a linear ($z$) spatial winding. By contrast, if one considers the application of a single frequency-swept pulse executing a certain manipulation of the spins throughout the sample (excitation, inversion) while in the presence of a constant gradient $G_e$, a quadratic $z^2$-dependent contribution will also arise. This can be appreciated by considering a case whereby spins with a given off-resonance $\Omega$ are sequentially excited by a $\pi/2$ pulse sweeping a sample $L$ over a duration $t^{\max}$. At the conclusion of a sweep extending from $z_i \leqslant z \leqslant z_f$ spins will have accumulated an overall phase,

$$\phi(z) = \phi_o + (t^{\max}\Omega/L)z + (\gamma G_e t^{\max}/2)z + (\gamma G_e t^{\max}/2L)z^2. \tag{6}$$

This expression has a constant $\phi_o$ term which for simplicity we neglect, as well as the $(t^{\max}\Omega/L)z$ term containing the kind of helical chemical shift winding that is needed. In addition, it contains a gradient-induced offset of the kind already mentioned (and which can be compensated via coherence selection gradients, rf offseting, etc.) plus a final gradient-derived term that, being quadratic in $z$, will not enable the collection of echoes via the usual $k$-driven unwinding. It is to eliminate this last term that all the encoding alternatives hitherto described incorporate a second frequency sweep acting during the course of a different $G_e'$ gradient. The reliance of the PR scheme on *two* indirect-domain manipulations opens up the opportunity of removing this problematic term by relying on the two separate stages of the experiment. Indeed this term is dependent on a gradient strength under our control but not on the unknown chemical shifts that one is trying to measure; the ultrafast-based 3D PR protocol can therefore be modified from the "dual-sweep" formats discussed above, into a sequence of the kind illustrated in Fig. 5(A). This variant contains a single frequency-swept rf pulse per indirect domain and individual gradient strengths $G_e^1$ and $G_e^2$ associated with these sweeps that are now calibrated to cancel out each other's quadratic components. On the basis of Eq. (6) this equates requesting

$$\gamma_1 G_e^1 t_1^{\max} + \gamma_2 G_e^2 t_2^{\max} = 0. \tag{7}$$

Given that the PR requirements will demand, as before, that the overall encoding times $t_1^{\max}$, $t_2^{\max}$ be varied systematically as $\cos\alpha$, $\sin\alpha$ in order to monitor the desired set of $\alpha$ projections, this means that the undesired quadratic contributions will cancel each other out by setting $G_e^1 = G_e \sin(\alpha)/\gamma_1$, $G_e^2 = -G_e \cos(\alpha)/\gamma_2$.

Issues that in connection with these various conditions are worth highlighting include: (i) Eq. (7) only defines a ratio between the gradients to be used for a given $\alpha$ value, yet their overall strength still remains under experimental control. (ii) For a homonuclear $\gamma_1 = \gamma_2$ case these conditions imply that a gradient-derived shift $\gamma G_e^1 \cos\alpha \sin\alpha\,(z_f^1 - z_f^2)$ will offset the indirect-domain peaks in all spectra, $z_f^{1,2}$ denoting the final spatial coordinate addressed by each sweep. This offset is known and should be corrected or factored in by the PR process. (iii) The reliance of this approach on the use of two different domain gradients will prevent the acquisition of "pure" $F_1F_3$ or $F_2F_3$ projections but not of nearby $\alpha$ traces. (iv) As in the cases discussed above this new single-gradient approach is well suited for selecting different signs in the encoding coefficients $C_1, C_2$ by relying on the relative directions of the sweeps employed to affect the encoding. (v) The arguments pertaining Eqs. (6) and (7) are based on $\pi/2$-pulse manipulations but can be extended to incorporating one or more $\pi$-based rf sweeps by considering that spatial encoding effects "double" upon considering spin inversions vis-à-vis spin excitations/storages.

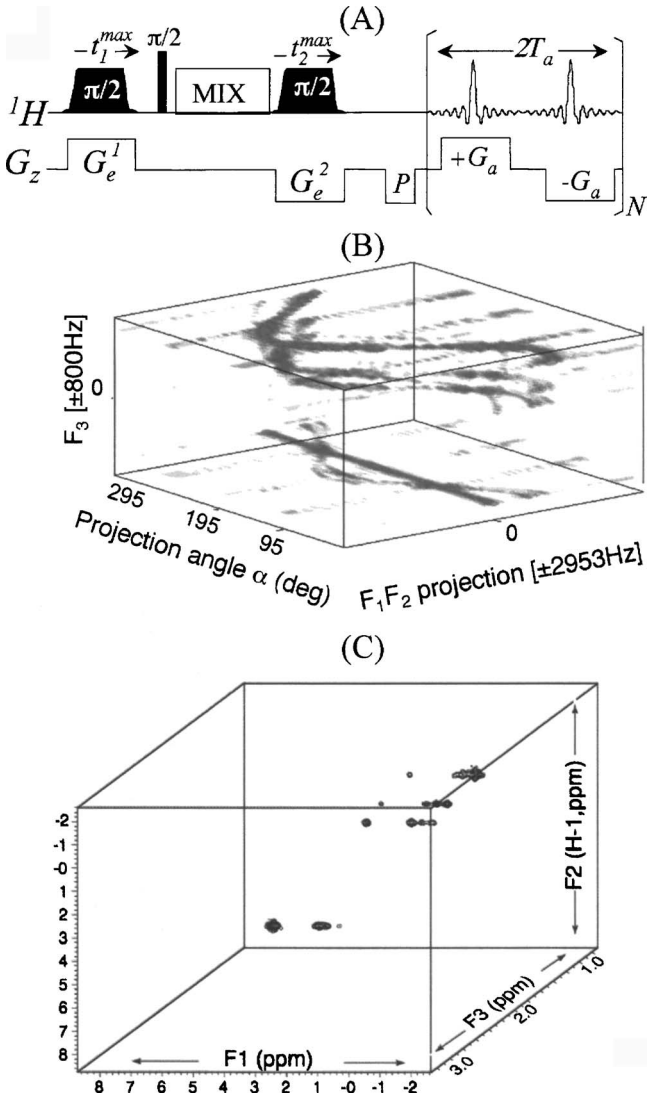


FIG. 5. Example of a "single sweep" version of the ultrafast 3D PR experiment. (A) $^1$H homonuclear 3D sequence incorporating a TOCSY mixing between the $t_1$ and $t_2$ periods. A given $\alpha$ angle is defined by adjusting the durations of the frequency-swept rf pulses according to $t_1^{\max} = t_{\text{ind}}^{\max}|\cos(\alpha)|$ and $t_2^{\max} = t_{\text{ind}}^{\max}|\sin(\alpha)|$, while gradients strengths are tuned to create a $z^2$-free spatial evolution by keeping $G_e^1 = G_e \sin(\alpha)$, $G_e^2 = -G_e \cos(\alpha)$. The usual $P$ gradient pulse was also added. (B) Full rotation plot arising from an $n$-butylchloride/$CDCl_3$ sample, showing for each peak in $F_3$ its expected sinusoidal trajectory. (C) 3D spectrum reconstructed using four projections at $\alpha = \pm 25°, \pm 45°$—each of these collected within a single scan. Experimental parameters: $t_{\text{ind}}^{\max} = 10$ ms, $G_e = 10$ G/cm, $T_a = 300$ $\mu$s, $G_a = 20$ G/cm, 60 ms DIPSI-2 mixing.

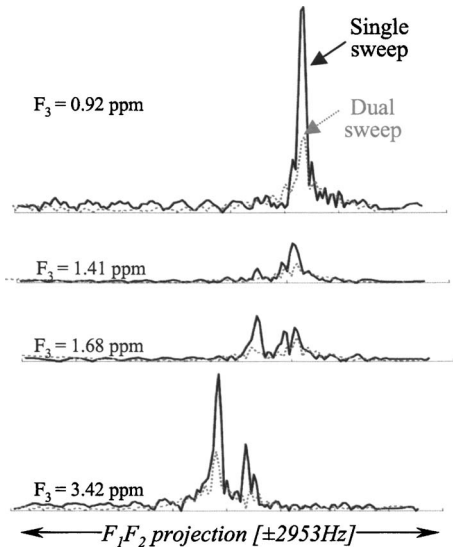


FIG. 6. Comparison between one-dimensional traces extracted for the different indicated sites of an *n*-butylchloride/$CDCl_3$ solution, from the $\alpha=45°$ projection of a $t_{ind}(t_1)$-TOCSY-$t_{ind}(t_2)$-$t_3$ 3D PR experiment. Dotted red lines represent traces collected using separate dual-sweep excitation blocks of the kind introduced in Fig. 3, whereas solid black lines relied on single sweeps for encoding the indirect domains. Shared experimental parameters of both experiments include $t_{ind}^{max}=10$ ms with $t_1=t_2=t_{ind}^{max}\cos(45°)$, $G_a=25$ G/cm, $T_a=300$ $\mu$s, $N=128$, 40 ms DIPSI2 mixing. For the dual-sweep excitation experiment a sequence of the kind shown in Fig. 3 was used with $G_e=10$ G/cm, $G_e=50$ G/cm with duration according to $t_{ind}^{max}\sin\alpha/10$, $G_e^1=10$ G/cm, $G_e^2=5$ G/cm. For the single sweep experiment (Fig. 5): $G_e=10$ G/cm with $G_e^1=-G_e^2=G_e\cos(45°)$. All data are shown in an equal absolute intensity mode.

In order to test the performance of this new PR-oriented encoding approach homonuclear tests like the ones reported in Fig. 3 for an *n*-buthylchloride/$CDCl_3$ solution were repeated, using single rf $\pi/2$ pulse sweeps under the above-mentioned conditions for characterizing each of the indirect domains. Like in the earlier examples a TOCSY-type mixing was inserted, this time in-between the $t_1$ and $t_2$ periods. A representative $\alpha$-rotation plot of the resulting 2D single-scan NMR spectra is presented in Fig. 5(B), achieved by suitable manipulations of the $t_1^{max}$, $t_2^{max}$ and $G_e^1$, $G_e^2$ parameters. Note that for each $F_3$ resonance peak along the two orthogonal indirect domains describe the expected $\Omega_1\cos(\alpha)+\Omega_2\sin(\alpha)$ sinusoidal trajectory and that, even though the orthogonal $\alpha=0°$ and 90° projections are not detectable by this scheme, spectra at $\alpha=5°$ and 85° show a good approximation to the pure 2D spectra expected along the $F_1F_3$ and $F_2F_3$ planes. The full 3D spectrum can still be reconstructed using a very small number of projections; Fig. 5(C) illustrates this for traces chosen at ±25°, ±45°, giving an experimental time for the full 3D NMR acquisition of 8 s. But most important, the relatively few manipulations involved give this approach a sensitivity advantage over the concatenated frequency-swept strategies illustrated earlier; for instance, under identical resolution and spectral width conditions, the approach introduced in Fig. 5 exhibits over twice the sensitivity of its counterpart in Fig. 3 (Fig. 6).

## IV. DISCUSSION AND CONCLUSIONS

The present study introduced and demonstrated a number of approaches merging projection-reconstruction and spatial encoding ideas that can compress the sampling needs of 3D NMR acquisitions to just a few seconds. The rationale behind this merging was to exploit the strong point of PR NMR, which approaches the acquisition of *n*D NMR spectra from the standpoint of back projecting a reduced number of 2D data planes, and couple into it the significant time saving offered by ultrafast NMR for collapsing the time required by each of these 2D acquisitions down to a single NMR scan. This enables one to complete the 3D data acquisition process within very few scans and, while it could be argued that the resulting experiment is still "slow" versus ultrafast 3D acquisitions based on a full spatial encoding,[21] it is characterized by a higher per-scan sensitivity and it no longer demands the availability of multiple orthogonal gradients. It is also clear that the ultrafast backprojection principles hereby presented for 3D NMR can be extended in a straightforward fashion to PR experiments of higher ($n\geqslant 4$) dimensionalities, simply by translating the temporal incrementation conditions of these experiments into spatiotemporal terms—always while relying on the use of a single-axis gradient encoding. Achievable spectral resolution and bandwidth considerations in these extended experiments should in principle be similar to those arising in conventional PR acquisitions.

Standing in juxtaposition to the significant speedup that ultrafast PR brings to 3D NMR, are the sensitivity limitations that may also be associated with this new approach. One of these relates to the intrinsic noise increase arising in gradient-based ultrafast *n*D experiments, whose manifestation in 2D NMR acquisitions has been discussed elsewhere.[19,28] In the present case such noise penalties may become aggravated, owing to the additional coherent and incoherent signal losses that occur upon extending two-dimensional pulse sequences into a third dimension. Moreover, whereas conventional 3D NMR acquisitions offset such penalties in part by the introduction of an additional time parameter associated with a multiscan signal averaging, such multiplexing advantages are not necessarily exploited by accordion-based *n*D reconstruction methods. Thus, for example, the lowest-value algorithm[17]—although fast, reliable, and of good overall performance—does not exploit the combination of multiple 2D projections to improve the overall sensitivity of the final 3D NMR data. Each individual ultrafast 2D acquisition would therefore need a sufficient quality to discern all the peaks to be correlated, prior to their combined 3D processing. On the other hand, the CLEAN algorithm used throughout this work,[29] as well as alternative PR protocols,[30] are more involved than the minimum value algorithm but enjoy the multiplex advantage and thus can help overcome the sensitivity limitations of individual 2D ultrafast acquisitions. Reliance on such algorithms is preferred when examining solutions in the low mM (or sub mM) regime.

We believe that the present study successfully exemplifies the opportunities that may arise when viewing the alternatives that have emerged over the last few years for accelerating multidimensional NMR acquisitions as involving complementary, rather than competing, concepts. Such "hybridization" of methodologies may result in immediate practical benefits, as exemplified by the speeded-up 3D PR ex-

periments illustrated in Figs. 2–4. They may also open up spectroscopic opportunities that are simply unavailable when considering each of its constituents separately, for instance, the availability of space as a new physical variable susceptible to be "accordioned" with either positive or negative signs, or the single sweep spatial encoding alternative introduced in Sec. III C. We believe that further valuable opportunities rest at the intersection of other various methods being developed to accelerate and optimize *n*D NMR acquisitions; we trust to report on some of these in upcoming studies.

## ACKNOWLEDGMENT

This work was supported by the Israel Science Foundation (ISF 1206/05).

[1] E. Becker, *High Resolution NMR* (Academic, New York, 2000).
[2] J. Cavanagh, W. J. Fairbrother, A. G. Palmer, and N. J. Skelton, *Protein NMR Spectroscopy: Principles and Practice* (Academic, San Diego, 1996).
[3] J. Jeener, *Ampere International Summer School II*, Basko Polje, Yugoslavia, 1971 (unpublished).
[4] W. P. Aue, E. Bartholdi, and R. R. Ernst, J. Chem. Phys. **64**, 2229 (1976).
[5] C. Griesinger, O. W. Sorensen, and R. R. Ernst, J. Magn. Reson. (1969-1992) **84**, 14 (1989).
[6] R. R. Ernst and W. A. Anderson, Rev. Sci. Instrum. **37**, 93 (1966).
[7] E. Kupče, T. Nishida, and R. Freeman, Prog. Nucl. Magn. Reson. Spectrosc. **42**, 95 (2003).
[8] H. S. Atreya and T. Szyperski, Methods Enzymol. **394**, 78 (2005).
[9] V. A. Mandelshtam, J. Magn. Reson. **144**, 343 (2000).
[10] J. C. Hoch and A. S. Stern, Methods Enzymol. **338**, 159 (2001).
[11] Y. Orekhov, I. Ibraghimov, and M. Billeter, J. Biomol. NMR **27**, 165 (2003).
[12] R. Brüschweiler and F. Zhang, J. Chem. Phys. **120**, 5253 (2004).
[13] E. Kupče and R. Freeman, J. Magn. Reson. **162**, 158 (2003).
[14] G. Bodenhausen and R. R. Ernst, J. Magn. Reson. (1969-1992) **45**, 367 (1981).
[15] T. Szyperski, G. Wider, J. H. Bushweller, and K. Wuthrich, J. Am. Chem. Soc. **125**, 9307 (1993).
[16] S. Kim and T. Szyperski, J. Am. Chem. Soc. **125**, 1385 (2003).
[17] E. Kupče and R. Freeman, J. Am. Chem. Soc. **126**, 6429 (2004).
[18] L. Frydman, T. Scherf, and A. Lupulescu, Proc. Natl. Acad. Sci. U.S.A. **99**, 15858 (2002).
[19] L. Frydman, T. Scherf, and A. Lupulescu, J. Am. Chem. Soc. **125**, 9204 (2003).
[20] K. Nagayama, P. Bachmann, K. Wüthrich, and R. R. Ernst, J. Magn. Reson. (1969-1992) **31**, 133 (1978).
[21] Y. Shrot and L. Frydman, J. Am. Chem. Soc. **125**, 11385 (2003).
[22] Y. Shrot, B. Shapira, and L. Frydman, J. Magn. Reson. **171**, 162 (2004).
[23] P. Pelupessy, J. Am. Chem. Soc. **125**, 12345 (2003).
[24] A. Tal, B. Shapira, and L. Frydman, J. Magn. Reson. **176**, 107 (2005).
[25] N. S. Andersen and W. Köckenberger, Magn. Reson. Chem. **43**, 795 (2005).
[26] J. Keeler, *Understanding NMR Spectroscopy* (Wiley, New York, 2006), Chap. 11.
[27] L. E. Kay, P. Keifer, and T. Saarinen, J. Am. Chem. Soc. **114**, 10663 (1992).
[28] B. Shapira, A. Lupulescu, Y. Shrot, and L. Frydman, J. Magn. Reson. **166**, 152 (2004).
[29] E. Kupče and R. Freeman, J. Magn. Reson. **173**, 317 (2005).
[30] J. W. Yoon, S. Godsill, E. Kupče, and R. Freeman, Magn. Reson. Chem. **44**, 197 (2006).
[31] S. Rucker and A. J. Shaka, Mol. Phys. **68**, 509 (1989).